Acta Materialia 127 (2017) 108–116

Contents lists available at ScienceDirect

Acta Materialia

journal homepage: www.elsevier.com/locate/actamat

Full length article

Tuning the nanoscale morphology and optical properties of porous gold nanoparticles by surface passivation and annealing

Anna Kosinova [a], Dong Wang [b], Eszter Baradács [c], Bence Parditka [c], Thomas Kups [b], Leonid Klinger [a], Zoltán Erdélyi [c], Peter Schaaf [b], Eugen Rabkin [a, *]

[a] Department of Materials Science and Engineering, Technion – Israel Institute of Technology, 32000 Haifa, Israel
[b] Chair Materials for Electronics, Institute of Materials Science and Engineering and Institute of Micro- and Nanotechnologies MacroNano®, TU Ilmenau, Gustav-Kirchhoff-Str. 5, 98693 Ilmenau, Germany
[c] Department of Solid State Physics, University of Debrecen, P.O. Box 2, H-4010, Debrecen, Hungary

ARTICLE INFO

Article history:
Received 4 July 2016
Received in revised form
7 January 2017
Accepted 8 January 2017
Available online 10 January 2017

Keywords:
Coarsening
Diffusion
Nanoporous gold
Plasmon resonance
Thermodynamic stability

ABSTRACT

We synthesized the arrays of porous gold nanoparticles attached to a fused silica and SiO_2/Si substrates employing a combination of thin film solid state dewetting and dealloying methods. We demonstrated that the surface of porous gold nanoparticles can be passivated with a thin and conformal alumina layer produced by the plasma-enhanced atomic layer deposition method. This passivation results in significant improvement of the thermal stability of the nanoporous morphology. Whereas as–produced porous gold nanoparticles start to coarsen at the temperature as low as 160 °C, their passivated counterparts are thermally stable up to 800 °C. At higher temperatures, the solid gold nanoparticles are formed on the outer surfaces of the passivated porous gold nanoparticles, leaving behind partially emptied alumina shells. We correlated the optical absorbance spectra of the as-produced and annealed particles with their morphology and microstructure. A broad absorption peak in the infrared region was associated with thin gold ligaments of 10–15 nm in diameter, and coarsening of these ligaments in the unpassivated particles has led to the attenuation of the peak. The passivated particles demonstrated the stability of the infrared absorption intensity up to the formation of solid gold nanoparticles at 900 °C, and the red shift of the visible-range plasmon resonance peak above 600 °C. We conclude that surface passivation and heat treatments represent efficient tools for tuning surface plasmon resonance properties of porous gold nanoparticles.

1. Introduction

A wide range of applications of metal nanoparticles relies on the phenomenon of surface plasmon resonance. Gold nanoparticles are the classical example of the system exhibiting surface plasmon resonance, which originates from the collective oscillation of electrons in the conduction band in response to optical excitation [1]. This induces very strong surface electromagnetic fields, which are especially useful in chemical sensors and biodetectors, surface enhanced Raman scattering [2], wavelength filters, and in other applications.

It is known that interaction of metal nanoparticles with light depends greatly on the morphology, dimensions and dielectric environment of nanoparticles. Variations in configuration and chemical composition of metal nanoparticles allow tailoring their plasmonic properties [3] and other functionalities [4].

The formation of interconnected porosity inside metal nanoparticles, which increases their surface-to-volume ratio, offers an opportunity for design of new surface and optical properties [5]. Different size of ligaments as well as the shape and size of the particles provide the surface plasmon resonance tunability over a wide range of wavelengths. It has been shown that the average near-field intensity enhancement in porous Au nanoparticles dispersed in aqueous solution was about 10 times higher than in the solid particles [6]. Though a number of publications on plasmon properties of different types of gold nanostructures (including nanoporous gold membranes) are available in the literature [7–10], only few studies report the optical performance of three-dimensional porous Au nanoparticles [6,11].

Typically, the methods for optical sensor fabrication include

* Corresponding author.
E-mail address: erabkin@tx.technion.ac.il (E. Rabkin).

http://dx.doi.org/10.1016/j.actamat.2017.01.014
1359-6454/

several steps and rely on assembling of solution-synthesized metal nanoparticles on a substrate [12,13]. The lithography-based methods are widely used to fabricate well-defined nanostructures [14,15], but technical complications, high costs and low scalability stimulate the development of other methods. Solid-state dewetting of a thin metal film is the simplest and low-cost method for immobilization of nanoparticles in a self-assembly manner on a substrate [16], yielding the low dispersion of the characteristic inter-particle spacing. The dimensions of the nanostructure obtained by dewetting can be controlled by the initial thickness of a metal film [2]. Combined with other techniques, dewetting can be utilized to produce ordered periodic arrays of nanoparticles [17,18]. Porous gold nanoparticles (PGNs) produced by solid-state dewetting of Au-Ag films on the substrate with the subsequent selective etching of Ag [19] represent an attractive platform for surface enhanced Raman scattering. This processing technique, which was utilized in the present study, provides the nanoparticles with dimensions and particle spacing below the resonant wavelength required for the resonance excitation. The typical dimensions of the particles and pores are in the range of hundreds and just a few nanometers, respectively, which result in high capillary forces lowering the thermal stability of the particles. Due to the large total excess surface energy, nanoporous metals are inherently unstable against thermal coarsening [20], which is the main disadvantage preventing their applications at elevated temperatures or in chemically active environments [21]. The coarsening of PGNs has been studied in our recent *in-situ* and *ex-situ* experiments [22]. We observed the onset of thermal degradation of gold nanoporous structure at a relatively low temperature of about 160 °C [22]. In order to stabilize the morphology, it is important to hinder the surface diffusion. The most commonly used method to suppress surface diffusion and to improve the stability of nanoporous structure relies on alloying with small amounts of high melting point metals such as Pt or Pd. Incorporation of small concentration of Pd into nanoporous gold-based alloy was shown to contribute to high electrocatalytic activity and electrochemical stability of the alloy [23]. Small amounts of Pt added to the bulk of the precursor Ag/Au alloy was found to stabilize the morphology of the porous metal at elevated temperatures and in harsh chemical environments [24], which is due to lower diffusion coefficient of Pt compared to that of Au. At the same time, the nanoporous structure functionalized by Pt electrodeposited onto nanoporous gold surface significantly coarsened at 400 °C [25]. Another way to prevent thermal degradation of nanoporous structure is the surface passivation by a thermally stable oxide, such as silica, titania or alumina [26]. Among the mentioned metal oxides, alumina is expected to ensure the highest thermal stability of nanoporous morphology because it exhibits the highest crystallization temperature. Coarsening of nanoporous gold film passivated with TiO_2 was observed at about 600 °C, while Al_2O_3-coated film was stable up to 900 °C [26]. The latter coating also caused a significant increase of mechanical strength of the nanoporous Au film. We believe that the improved thermal stability of PGNs with Al_2O_3-passivated surface will result in stabilization of optical properties, thus enabling to expand the range of practical application of PGNs to higher temperatures. Plasma-enhanced atomic layer deposition (ALD) is the most appropriate technique for depositing of a few nanometers thick, homogeneous and conformal coatings. Therefore, we employed the ALD technique to cover PGNs with amorphous alumina passivation layer.

The objective of the present research is two-fold: firstly, we aim at establishing the correlation between the nanoscale morphology and optical properties of PGNs; secondly, we intend to enhance the thermal stability of PGNs and stabilize their optical properties by means of deposition of amorphous oxide layer. Moreover, understanding the microstructure evolution of the PGNs "packaged" in an inert rigid shell is interesting from the fundamental point of view, and may open new avenues of the fine-scale materials processing. Indeed, the morphology and microstructure changes in such nanoparticles are a result of synergetic interplay of the capillary- and thermal expansion mismatch-induced internal stresses, of the mechanical behavior of the thin amorphous alumina shell, and of the bulk, surface, and interface self-diffusion of gold. The present research explores the possibility of designing a surface plasmon resonance material supported by a substrate relevant for surface enhanced Raman scattering, which can effectively operate at elevated temperatures. The manipulation of the metal surface passivation conditions offers the possibility for tailoring the nanoscale morphology of PGNs and fine-tuning the plasmon resonance frequency.

2. Experimental

2.1. Sample preparation

Au/Ag bi-layer films (8 nm Au/20 nm Ag) were deposited on SiO_2/Si substrates and on glass (fused silica) substrates using electron beam evaporation. Prior to deposition on the Si substrate, 200 nm thermal SiO_2 layer was grown in order to prevent the reaction between the substrate and the films deposited on it. Firstly, the dewetting annealing of the bi-layer films was performed at 900 °C in Ar flow for 15 min, and as a result Au/Ag alloy nanoparticles were formed. Afterwards, nanoporous gold nanoparticles were formed by the selective removal of Ag from the alloy nanoparticles in a nitric acid: the samples were submerged in a 65 wt% HNO_3 aqueous solution at 21 °C for 5 min.

5-nm thick Al_2O_3 films were coated onto the as-dealloyed samples by means of plasma-enhanced atomic layer deposition in a Beneq TFS 200 type ALD reactor. Trimethyl aluminium and oxygen plasma were used as the precursor materials for the Al_2O_3 deposition at 150 °C. The ALD growth cycle consisted of the following steps: 450 ms trimethyl aluminium dose at 1 mbar chamber pressure, 3 s of nitrogen purge, 6 s of oxygen plasma at 50 W power, 3 s of nitrogen purge. The growth rate of the layers was 1.43 Å/cycle. Accordingly, the growth cycle was repeated 35 times to deposit 5-nm thick Al_2O_3 layer.

As-prepared samples were annealed in a quartz tube resistance furnace in an ambient air in the temperature range from 350 to 1000 °C. The duration of each annealing cycle was 60 min.

We also prepared a reference sample from the 25 nm thick Au film on sapphire substrate. The film was dewetted at 900 °C in ambient atmosphere for 90 min in order to obtain isolated gold particles. Afterwards, 5-nm thick ALD alumina layer was coated onto the solid gold particles. We used the same ALD-deposition conditions as were used for the porous particles. The annealing conditions used for the reference sample were also identical to those employed for the samples of unpassivated PGNs and Al_2O_3-passivated PGNs.

2.2. Sample characterization

The morphology evolution was tracked after each heat treatment by means of high-resolution scanning electron microscope (HRSEM, Zeiss Ultra Plus). HRSEM micrographs were taken using a secondary electron detector, at an acceleration voltage of 3 kV for the samples supported by SiO_2/Si substrates and for the reference sample. Use of a low voltage and fixing the samples on a conductive stage prevented the charging of nonconductive substrates. The chemical composition was measured via energy-dispersive spectroscopy (EDS), which was used in association with HRSEM. EDS

was performed using an acceleration voltage of 5 kV, a probe current of 0.3 nA, and a working distance of 8.5 mm. The take-off angle of X-ray radiation was 35°. Acquisition time was 40 s per a single measurement.

Transmission electron microscopy (TEM) images and electron diffractions were obtained using TEM (FEI Tecnai 20s-twin) operated at 200 kV. The TEM lamellar was prepared by using the milling with focused ion beam (FIB, Carl Zeiss Auriga 60 crossbeam).

The microstructure evolution during thermal treatment was characterized employing the X-ray diffraction (XRD) system (Rigaku SmartLab) equipped with a high-temperature heating stage. The measurements were performed in a parallel beam configuration, and monochromatization of the beam was performed using a 2-bounce Ge(220) monochromator. In-situ XRD data were collected throughout the annealing from 350 °C to 900 °C. The measurements were carried out on the samples supported by SiO_2/Si substrates. The diffraction patterns were recorded in θ-2θ scanning mode using Cu K_α radiation ($\lambda = 1.5406$ Å) in the range of 2θ between 37° and 39°.

Samples supported by glass substrates were used for optical measurements. The glass is characterized by high optical transparency (about 95%) in the spectral range 200–2100 nm. Transmission and reflection spectra were measured in the wavelength range of 350–1100 nm using a double beam scanning UV–vis–NIR spectrophotometer (Cary 5000, Agilent) equipped with an integrating sphere. Afterwards, the absorption was calculated from the measured spectra.

3. Results and discussion

3.1. Morphology and microstructure

As-deposited Au and Ag films exhibited strong [111] texture, which was inherited by solid alloy nanoparticles and, correspondingly, by porous gold nanoparticles. During dewetting of the bilayer films at a temperature of 900 °C, the grains in the film grow to such an extent that only single crystalline alloy particles are obtained. As-dealloyed nanoparticles retain their single crystalline character and exhibit three-dimensional bi-continuous structure with pore dimensions of about 20 nm (Fig. 1a). The average diameter of PGNs is 300 nm. The particles coated with amorphous alumina layer retain the original open porosity, since the alumina thickness is 5 nm. ALD-modified PGNs (APGNs) exhibit uniform alumina coating both on the outer surface and inside the pores (Fig. 1b). The selected area electron diffraction was taken from the sample after dealloying and coating with Al_2O_3. It shows a diffraction pattern characteristic of a single crystalline gold (insert in Fig. 1b).

Fig. 2 shows the morphology evolution of APGNs annealed in the temperature range 350–800 °C. At the annealing temperature of 350 °C no morphology changes are observed. After the heat treatments at 500 °C and 600 °C nanoparticles were also stable, but the detailed examination revealed the contrast change of individual ligaments in SEM images (Fig. 2c and d), which was caused by a slow diffusion of gold along the alumina layer. EDS spectra confirm the absence of gold in these dark features (Fig. 3). The following heating up to 800 °C results in the increased number of dark ligaments due to the increase of diffusion rate of gold atoms (Fig. 2e and f). Yet, a large part of nanoparticles preserves their structural integrity. The ligament size does not change with the annealing temperature.

The APGNs exhibited stable morphology up to 900 °C, but at such a high temperature fast surface and bulk diffusion of gold atoms promote the formation of solid gold nanoparticles, which is confirmed by EDS spectrum (Fig. 4c). Gold emerges from the

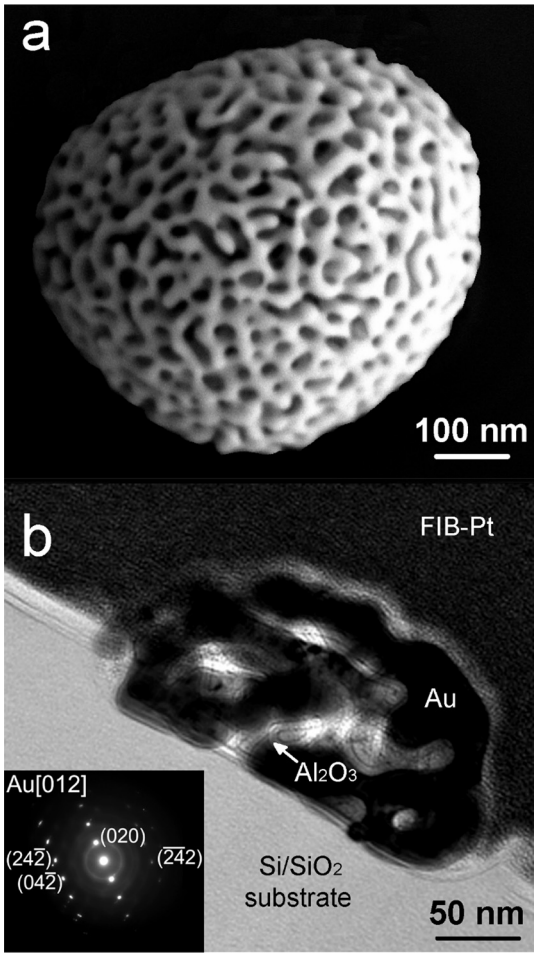

Fig. 1. (a) HRSEM micrograph of PGN on SiO_2/Si substrate, (b) TEM image of PGN coated with alumina. The inset electron diffraction pattern in (b) taken from the whole particle along the [012] zone axis confirms the single crystalline nature of APGN.

alumina coating leaving behind the hollowed alumina shell. As a result, faceted nanometer-sized Au crystals form on the surface of almost every incipient porous particle (Fig. 4a and b). Typically, one solid gold particle is formed from one porous particle. The size of the formed gold nanoparticles after annealing at 1000 °C lies in the range from 50 to 200 nm, with 60% of the particles being narrowly dispersed in size, from 100 to 150 nm (Fig. 4d). It is interesting to note that the emptied alumina shell retains the initial porous structure.

Continuous and smooth alumina coating serves as a passivation layer, effectively suppressing coarsening of porous gold nanostructure and hindering diffusion of gold atoms. At high temperatures, the alumina coating becomes highly strained due to the mismatch of thermal expansion coefficients of gold and alumina. This may result in cracks formation and partial delamination of the alumina layer. Gold starts to diffuse out from these defect sites in alumina. The driving force for this outdiffusion is the decrease of the total energy of all surfaces and interfaces in the system. Indeed, since the energy of gold-alumina interface is larger than the surface energy of alumina [27], emptying the porous alumina shell from gold results in decrease of surface and interface energy, duly compensating the increase of energy associated with the formation of new surfaces of solid gold nanoparticles. The mechanism for improvement of thermal stability by means of a passivation layer is related to the slower metal self-diffusion along the metal-ceramic

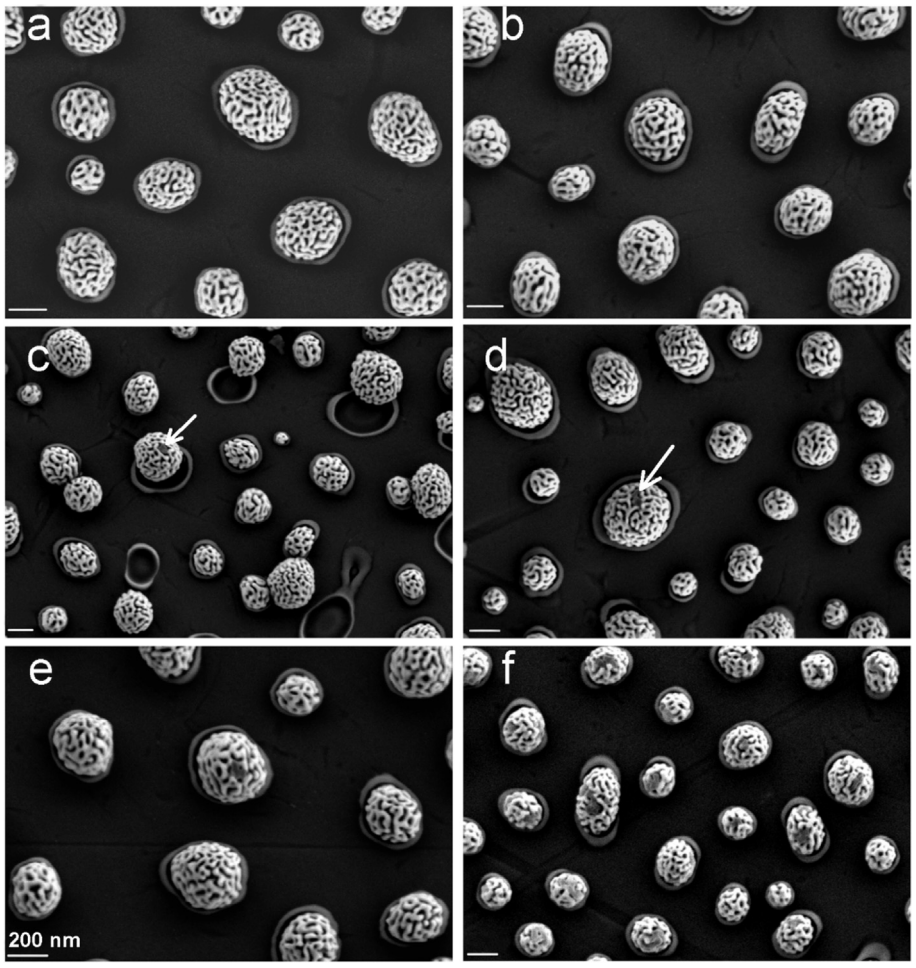

Fig. 2. HRSEM images of APGNs: (a) as-prepared, annealed for 60 min at (b) 350 °C, (c) 500 °C, (d) 600 °C, (e) 700 °C, (f) 800 °C. Arrows in (c) and (d) indicate contrast change of individual ligaments.

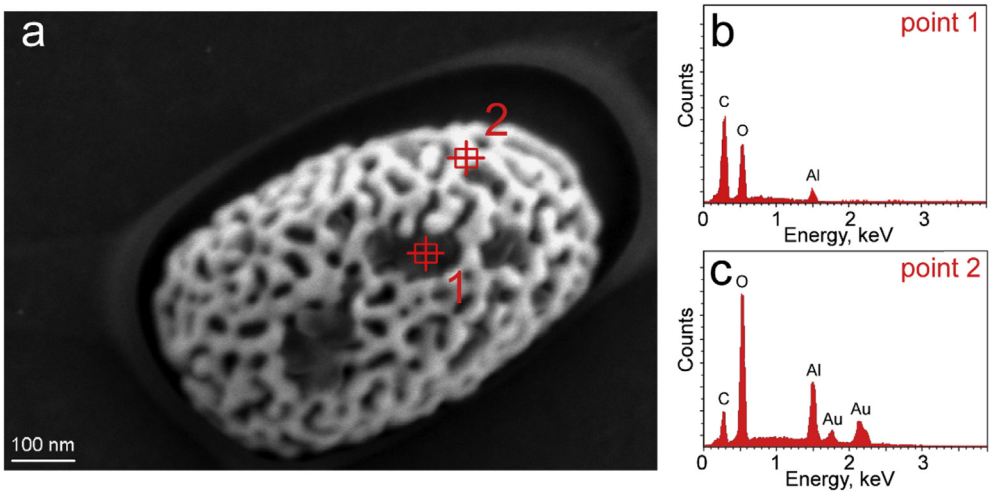

Fig. 3. (a) HRSEM image of the APGN annealed at 600 °C, and (b,c) corresponding EDS spectra acquired from the (b) dark and (c) bright regions in (a).

interface as compared with the surface self-diffusion [28].

It should be noted that the acceleration of morphology evolution of the APGNs above 900 °C cannot be attributed to the partial melting of the particles due to Gibbs–Thomson effect. Indeed, the size-dependent reduction of the melting point of Au nanoparticles was observed for the particles smaller than 10 nm in diameter [29]. The ligament size in APGNs synthesized in the present work is larger than 10 nm, which excludes the possibility of partial melting at the temperatures of 900 and 1000 °C.

The formation of a solid gold nanocrystal from a porous one

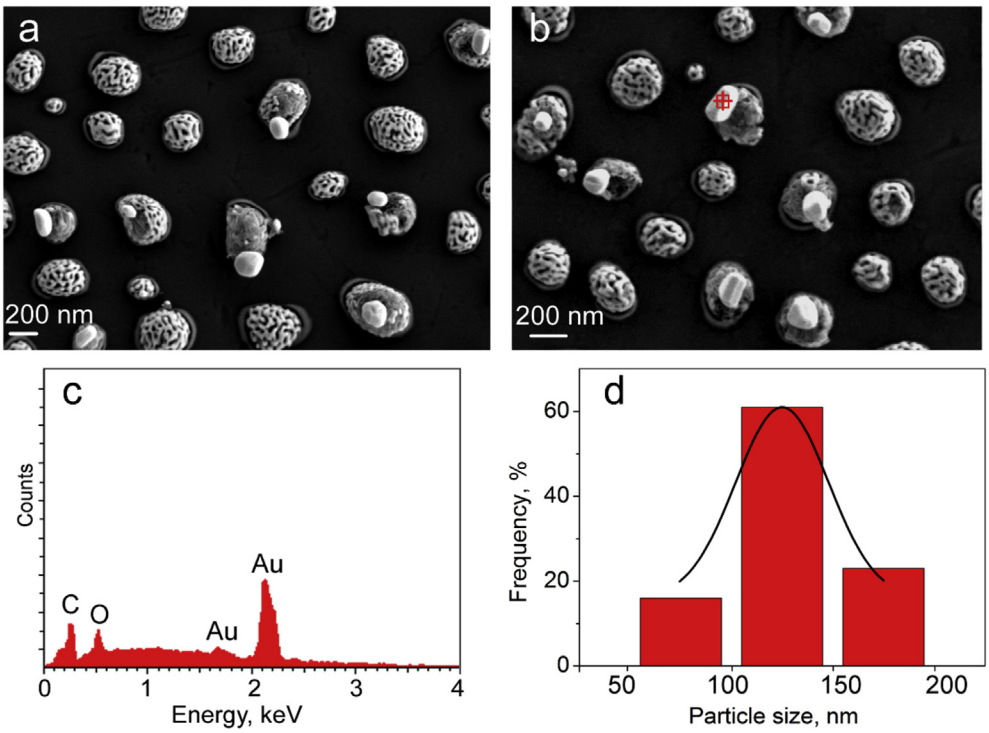

Fig. 4. HRSEM image of APGNs annealed at (a) 900 °C and (b) 1000 °C, (c) EDS spectrum acquired from the particle marked in (b); (d) particle size distribution after annealing at 1000 °C. Fitting curve is superimposed on the histogram.

relies on the diffusion of gold atoms along the Au/alumina interface, and in the bulk of gold ligaments. The mismatch of thermal expansion coefficients of gold and alumina results in high tensile stresses in alumina shell once the particles are heated to high temperature. These stresses result in cracks formation in the shell, or in its partial delamination. The dark ligaments observed in Figs. 2c–f, 3a, and 4a-b exemplify such defects in alumina shell. The defect sites of the alumina layer serve as nucleation sites for solid gold nanoparticles. Such nuclei may form due to relaxation of high compressive stresses in gold ligaments. Once the size of the gold nuclei exceeds some critical value, it can continue growing by emptying the alumina-covered gold ligaments. We developed a simple model of the growth of a solid gold nanocrystal and estimated the critical radius of the nucleus (see Supplementary Information Fig. S1 for details). Our model results in the following equation for the growth rate of a solid particle:

$$\frac{dR}{dt} = \frac{\alpha D_2 \Omega}{2RkT} \frac{D_1 r^2 n}{D_1 r^2 n + \alpha D_2 l R} \left(\frac{\gamma_i - \gamma_s}{r} - \frac{\gamma_{Au}}{R} \right), \quad (1)$$

where R is the radius of the growing particle, r is the radius of a ligament, D_1 and D_2 are the effective diffusion coefficients of gold along the ligament and in the gold particle, respectively, l is variable diffusion distance along the ligament, n is the number of ligaments feeding the growing particle, γ_i and γ_s are the energies of the Au/Al_2O_3 interface and of the surface of amorphous Al_2O_3 layer, respectively, γ_{Au} is the surface energy of gold, Ω is the atomic volume, α is a numerical coefficient of the order of one which depends on the shape of the growing particle, and kT has its usual thermodynamic meaning.

This expression yields the critical radius of a seed $R_{cr} \approx 10$ nm, with larger gold particles exhibiting fast stable growth (Fig. 5a). The nuclei with a lower radius are unstable and should disappear. The supercritical nucleus can form at the site of local rupture of the alumina shell due to the plastic relaxation of the compressive thermal stresses in gold ligaments. The maximum size of the formed solid particle is restricted by the amount of gold in the initial APGN. Taking into account the average size of the initial particle of about 300 nm (see Supplementary Information), we obtained the maximum radius R_{max} of the formed nanocrystal of about 115 nm. Our estimate is in good agreement with the experimental data (Fig. 4d), and explains why the formed gold particles exhibit quite narrow range of sizes. The solution of Equation (1) in the range of $R_{cr} < R < R_{max}$ yields the time of the particle formation. For example, the formation time of a particle with $R_{max} = 115$ nm at the annealing temperature of 1000 °C is only 120 s (Fig. 5b).

One of the main advantages of amorphous alumina is its high crystallization temperature. Indeed, crystallization of thin ALD alumina films has been reported at 900 °C [30] and at 1000 °C [31]. We performed the in-situ XRD annealing experiments of APGNs (see Section 3.2). X-ray diffraction patterns did not reveal any phase transformation from amorphous to crystalline alumina, despite the high annealing temperatures. We suppose that the reason for this stability of the amorphous structure is a high surface-to-volume ratio of the ALD-produced alumina layer. Due to the lower surface energy of amorphous alumina compared with γ- and α-crystalline polymorphs, this phase is energetically more favorable for specific surface areas exceeding 370 m^2/g [32], or $9.2 \cdot 10^8$ m^{-1} in the units of specific surface area per unit volume (the density of amorphous alumina is 2.5 g/cm^3). Gold ligaments provide a specific surface area of about 10^5 m^2/g ($1.9 \cdot 10^{12}$ m^{-1}) [19], thus thermodynamically stabilizing the amorphous alumina coating up to the temperature of 1000 °C.

In order to emphasize the uniqueness of the observed high-temperature behavior of APGNs, we prepared the reference sample of the ALD-passivated solid gold nanoparticles. Nanoparticles were obtained by solid state dewetting of 25-nm thick Au film on sapphire and afterwards were covered with 5-nm thick alumina

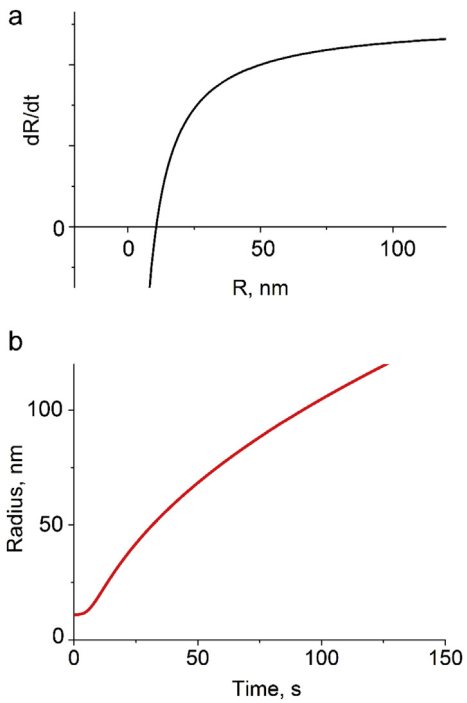

Fig. 5. (a) The dependence of the growth rate of a solid gold nanoparticle on its radius, and (b) the corresponding dependence of the nanoparticle radius on annealing time. The presented dependencies are given for the annealing temperature of 1000 °C.

layer. The annealing conditions were the same as for porous samples. The reference sample was morphologically stable up to 600 °C. At this temperature, we observed the formation of small bumps on the nanoparticle surface (Fig. 6a). At higher temperatures these bumps grew laterally, and simultaneously the new bumps on the initially featureless surfaces of gold nanoparticles were formed. The formation of these surface features is a result of gold diffusion inside a tight and conformal alumina shell. The gold atoms diffuse out from the edges of the particles due to the nucleation and growth of pores occurring at the corners of the particle/substrate interface. The thermodynamic driving force for this process is a relatively low surface energy of amorphous alumina (0.88 J/m^2) [33], and relatively high energy of the gold-alumina interface (2.15 ± 0.05 J/m^2) [27], which results in the formation of convex pores, and their expansion away from the corners of the gold particle. The material that diffused out of the pores accumulates in certain sites, which results in the formation of the surface bumps. In Fig. 6b we can clearly observe the emptied alumina shell, which outlines the boundaries of the initial particle. The excess pressure exerted by gold atoms accumulating in the surface bump results in exfoliation of the shell (Fig. 6b). The same processes take place at the temperature of 800 °C (Fig. 6c). The particles annealed at 900 °C exhibit substantial morphological changes (Fig. 6d) such as surface roughening and coarsening, which may indicate the crystallization of alumina shell. Thus, one can assume that ALD amorphous alumina coating on solid gold nanoparticles undergoes phase transformation at a lower temperature compared to the ALD coating on the PGNs.

3.2. Internal stresses

It is known that nanostructured materials exhibit high level of internal stress, which equilibrates the surface and interface stresses. Since the nanoporous microstructure formed after dealloying exhibits areas of high local curvature of varying sign, the existence of both tensile and compressive local stresses is expected in both PGNs and APGNs. At the same time, Weissmüller et al. have shown that the average bulk stress in the nanoporous structure is always compressive [34]. Because of their strong [111] texture, the PGNs obtained by solid state dewetting and dealloying represent a convenient object for testing the Weissmueller-Cahn theory. We have recently confirmed the compressive nature of internal stress in as-dealloyed PGNs [22]. Surface and interface diffusion of gold at a temperature of 350 °C was found to promote the coarsening of nanoporous structure and concomitant relaxation of the average compressive stress [22]. To clarify the effect of alumina coating on the internal stresses in APGNs, we performed the in-situ X-ray annealing experiments and tracked the position of the (111) Bragg reflection of gold. The experiments for PGNs and APGNs were performed under identical experimental conditions, the only difference being a much wider range of temperatures employed in the in-situ heating study of the APGNs.

As expected, increasing the temperature results in thermal expansion of the crystal lattice of gold, which causes a significant shift of the (111) reflection to the lower values of 2θ (Fig. 7). After cooling the sample back to room temperature, the diffraction peak shifts back exactly to its initial state. It is important to note a significant difference in the behavior of the diffraction peak in passivated and unpassivated PGNs. In the unpassivated PGNs, the initial position of the (111) reflection for the as-dealloyed particles was shifted to higher values of 2θ relatively to its nominal value for bulk gold. After the heating-cooling cycle, the peak did not return to its initial position, which indicated a decrease of compressive stresses in the PGNs due to the coarsening of their nanoporous structure [22]. The coincidence of the (111) Bragg reflection positions before and after in-situ annealing of APGNs means that alumina passivation layer stabilizes the initial nanoporous structure of the particles up to the highest temperature of 900 °C. The solid gold nanocrystals formed at high temperatures do not inherit the orientation of the APGNs and, hence, they do not contribute to the (111) diffraction peak. The gold remaining within the alumina shell after the heating-cooling cycle still exhibits the same average compressive stress as the as-received APGNs.

3.3. Optical properties

The samples used for optical measurements (on glass substrate) were annealed in the same temperature range (up to 1000 °C) as the samples supported by SiO_2/Si substrate. No difference in the morphology evolution of nanoparticles depending on the substrate was revealed. We correlated the changes of absorption spectra of passivated and unpassivated gold nanoparticles with their morphology evolution.

Absorption spectra of unpassivated PGNs before and after annealings are shown in Fig. 8. The absorption spectrum of the as-dealloyed sample shows two slight peaks in the visible region and a pronounced one in the near-infrared (IR) region (Fig. 8a, green curve). Short wavelength absorption is determined by the interzonal transitions in gold. This absorption manifests itself in the range of 350–500 nm as a slightly increased background. It does not depend on the morphology evolution of nanoparticles or on the changes in the surrounding media. Since the initial PGNs exhibit two different characteristic dimensions, we observed the optical response from gold nanoparticles, as well as from gold ligaments. The maximum distinguishable at 520 nm is due to the excitation of the optical plasmons in gold nanoparticles, whereas the prominent absorption band in the near-IR region ($\lambda_{max} = 980$ nm) is attributed to the plasmon oscillation modes in nanoscale ligaments. A similar structure of the absorption spectra has been reported for colloidal

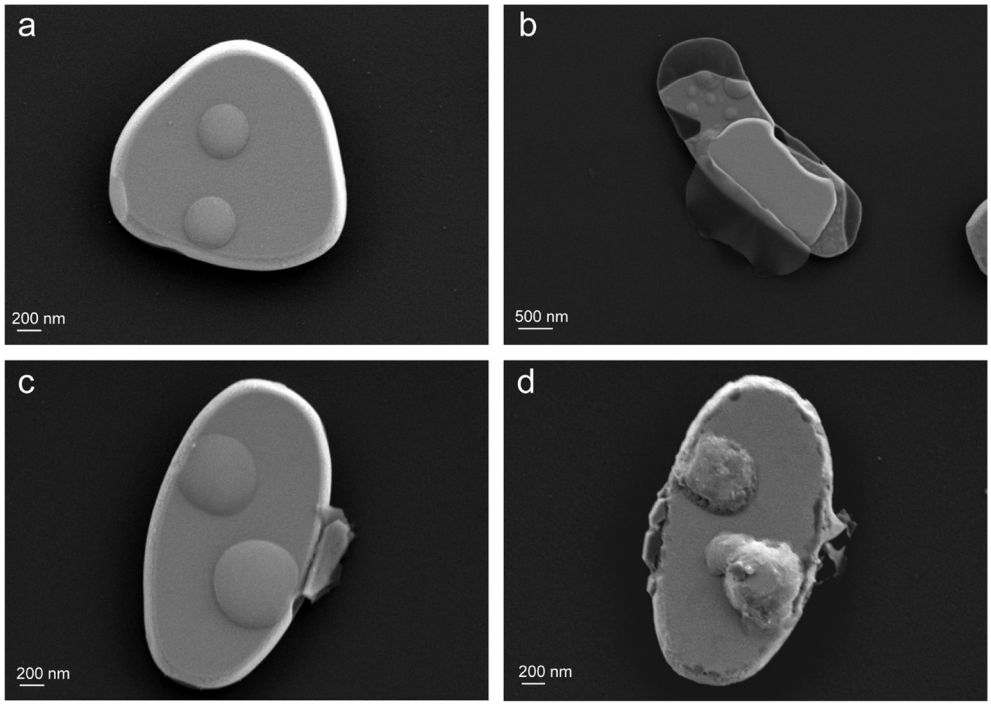

Fig. 6. HRSEM images of gold nanoparticles with ALD alumina coating annealed at (a) 600 °C, (b) 700 °C, (c) 800 °C, (d) 900 °C. (c) and (d) represent one and the same particle. The duration of each annealing cycle was 60 min.

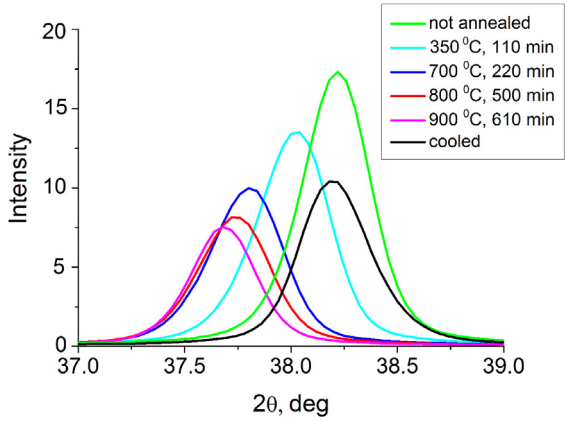

Fig. 7. The in-situ X-ray diffraction patterns of APGNs. The green and the black curves refer to APGNs prior and after the in-situ annealing experiment, respectively. (For interpretation of the references to colour in this figure legend, the reader is referred to the web version of this article.)

solutions of gold nanorods [35]. This wide absorption band can be considered as a convolution of individual narrow bands. It results from the multiple plasmonic contributions of interconnected gold ligaments and superposition of these resonances throughout the nanoparticles, which has been confirmed by the strong polarization effect [11].

The corresponding spectra of the annealed PGNs samples are considerably different. They show a rapid decrease and flattening of the IR absorption, followed by the increase of absorption intensity in the visible region. These spectral changes are observed right after the first annealing (Fig. 8a, cyan curve), which is accompanied by the corresponding changes in the nanoparticles morphology. We have shown in our recent work that open nanoporosity transforms into a metastable closed one upon heat treatment at 350 °C in air [22]. Surface diffusion promotes the thermal coarsening of ligaments, which occurs faster in the near-surface region. As a result, the annealed particles have a continuous outer surface with multiple concavities and a large pore inside the particle or at the particle/substrate interface. With increasing temperature the size of the closed pores decreases, which results in further lowering of IR intensity (Fig. 8a, blue and black curves). As the particles approach their equilibrium shape, the IR absorption band totally disappears (Fig. 8a, red curve).

A remarkable feature of the absorption spectra in Fig. 8 is the increase of absorption intensity in the visible region with coarsening of nanoporosity. As we can see from Fig. 8a, as-dealloyed PGNs exhibit a minor absorption peak at 520 nm. It becomes more pronounced with annealing-induced coarsening of PGNs. Such a variation of absorption intensity can be explained by the tendency of fine-porous structure to damp the plasmon peak at 520 nm due to electron-surface scattering [36]. Indeed, this surface plasmon band was essentially unidentifiable for gold crystallites of less than 2 nm in effective diameter, re-appearing for larger particles, with the intensity increasing with increasing crystallite diameter [37]. Also, there is some analogy in the behavior of gold plasmon peak observed in the present study, and in the study of the periodic structures of cylindrical holes in the composite film of P3HT:PMMA/Au [38]. Increase of the hole diameter at a fixed spacing between the holes resulted in the increase of the extinction intensity peak at 550 nm [38]. Assuming that there is some analogy between the hole diameter in Ref. [38] and the average pores diameter in the PGNs in the present study means that coarsening of the nanoporosity in the PGNs should result in the increase of the visible plasmon peak, in agreement with our experimental observations (see Fig. 8).

Fig. 8b shows the optical spectra of the APGNs. Due to the retention of open porosity in the passivated particles, they exhibit an optical response which is a superposition of the optical responses of the gold nanoparticles and of the interconnected

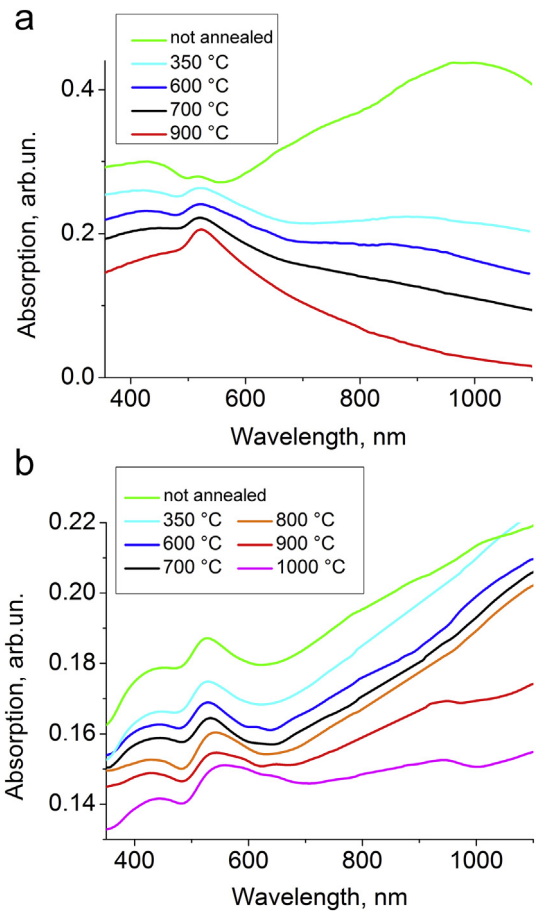

Fig. 8. Absorption spectra of (a) PGNs and (b) APGNs before and after heat treatments at different temperatures. Green spectra correspond to the samples before annealing. (For interpretation of the references to colour in this figure legend, the reader is referred to the web version of this article.)

ligaments (Fig. 8b, green curve). The IR plasmon peak shows a significant red-shift (by more than 100 nm) compared to its position in unpassivated particles. The absorption maximum lies beyond the studied spectral range. Such a significant shift is due to changes in the local refractive index around gold ligaments. Taking into account that the plasmon resonance frequency depends not only on the morphology of the particles, but also on the dielectric properties of the surrounding medium, the slightest change (only about 0.5%) [39] of the refractive index around nanoparticles will cause a detectable shift of the plasmon resonance peak. It has been shown that the excitation spectra can be effectively used to determine the variation of the dielectric constant of the medium within the pores and to detect the species adsorbed onto the surface of the pores [39]. The sensitivity of the plasmonic peak position to the refractive index of the surrounding medium was found to be much higher for hollow gold nanospheres than for their solid counterparts [40]. This is because both the inner and outer surfaces present in the hollow nanoparticles contribute to plasmonic resonance. Highly developed surface of the PGNs results in their increased sensitivity to the variations of the dielectric constant of the environment, so that even very thin ALD alumina coating causes a significant red-shift of the IR plasmon peak.

In contrast to the unpassivated particles, heat treatment of the APGNs does not result in a substantial spectral change. The stability of the IR band testifies to the thermal stability of the nanoscale structure. Only annealing at the temperatures of 900 and 1000 °C results in a significant attenuation of the red spectral tail, indicating the collapse of nanoporous structure.

The plasmon peak at $\lambda_{max} = 520$ nm in APGNs exhibits a slight red-shift after annealings at the temperature of 600 °C and above (Fig. 9). Below 600 °C, the position of this plasmon peak is stable. This is the same temperature at which the dark ligaments inside the particles appear in the SEM micrographs (see Figs. 2–3). The maximum red-shift of the plasmon peak ($\lambda_{max} = 555$ nm) was observed at the highest studied temperature of 1000 °C (Fig. 9). We also observed a distinct broadening of this absorption band and the appearance of a slight shoulder with increasing temperature (see Fig. 8b). All these features become essential at $T \geq 800$ °C and are related to the formation of small solid gold nanoparticles with elongated and irregular shape, which contribute to the overall absorption. The measured absorption is the integral absorption of particles of different sizes and shapes.

4. Conclusions

In conclusion, we synthesized the PGNs with thin conformal ALD alumina coating (APGNs) exhibiting excellent stability against coarsening at elevated temperatures. The deposition of amorphous alumina layer effectively suppresses the surface diffusion of gold up to the temperature of 900 °C, thus stabilizing the nanoscale morphology. Annealing at this and higher temperatures leads to the growth of solid gold nanoparticles leaving behind the emptied nanoporous alumina shell. We developed a kinetic model of the growth of solid nanoparticles and estimated the critical nucleus radius and the maximum radius of the formed particle. The obtained values are in a good agreement with the experimental results. We also demonstrated that the high level of capillary-induced internal compressive stresses in the passivated PGNs is preserved after prolonged annealing at 900 °C, indicating that some gold remains confined within the alumina shell.

We uncovered a strong correlation between the optical properties of PGNs and their morphology. The optical response of both as-dealloyed PGNs and as-received APGNs was found to be a combination of the responses of gold nanoparticles and of the smaller gold ligaments. Annealing of the PGNs results in coarsening of nanoporosity and concomitant damping of the near-IR plasmon peak in their absorption spectra. The morphological stability of APGNs at high temperatures results in the stability of their optical properties. Thus, we demonstrated that two plasmon bands inherent in PGNs could be stabilized up to the temperature of 900 °C by means of ALD of thin alumina layer. Moreover, the change of the dielectric environment around gold ligaments allows fine-tuning of the near-IR absorption. The improved thermal stability

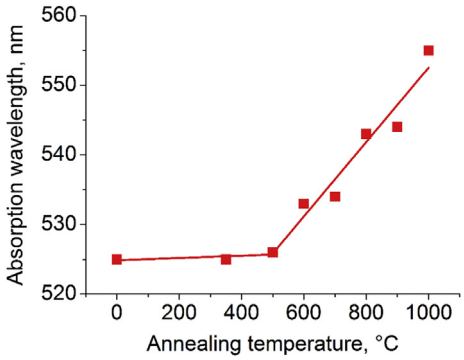

Fig. 9. The dependence of the visible-range plasmon resonance wavelength of the APGNs on annealing temperature.

and optical properties of alumina-stabilized PGNs opens the way for a number of promising applications at high temperatures and in chemically active environments, such as actuation and surface enhanced Raman scattering.

Acknowledgments

A.K. wishes to thank the Technion for the post-doctoral fellowship. This work was partially supported by the Deutsche Forschungsgemeinschaft (DFG, Grants SCHA 632/20-1 and SCHA 632/24-1), by the state of Thuringia (TMWAT, BioMacroNano 2020, 2010–2012; Grant B715-10009), by the OTKA Board of Hungary (No. NF101329) and by the GINOP-2.3.2-15-2016-00041. Helpful discussions with Prof. B. Pokroy, Dr. A. Berner and Mr. O. Kovalenko are heartily acknowledged. The authors are grateful to Ms. Diana Rossberg for the TEM sample preparation with FIB, and Mrs. Birgit Kolodziejczyk, Mrs. Ilona Marquardt, and Mr. Joachim Döll from TU Ilmenau for their help with samples preparation.

Appendix A. Supplementary data

Supplementary data related to this article can be found at http://dx.doi.org/10.1016/j.actamat.2017.01.014.

References

[1] K.A. Willets, R.P. Van Duyne, Localized surface plasmon resonance spectroscopy and sensing, Annu. Rev. Phys. Chem. 58 (2007) 267–297.
[2] M. Kang, S.-G. Park, Ki-Hun Jeong, Repeated solid-state dewetting of thin gold films for nanogap-rich plasmonic nanoislands, Sci. Rep. 5 (2015) 14790.
[3] R.P.M. Höller, M. Dulle, S. Thomä, M. Mayer, A.M. Steiner, S. Förster, A. Fery, C. Kuttner, M. Chanana, Protein-assisted assembly of modular 3D plasmonic raspberry-like core/satellite nanoclusters: correlation of structure and optical properties, ACS Nano (2016), http://dx.doi.org/10.1021/acsnano.5b07533.
[4] M. Hu, J. Chen, Z.-Y. Li, L. Au, G.V. Hartland, X. Li, M. Marquez, Y. Xia, Gold nanostructures: engineering their plasmonic properties for biomedical applications, Chem. Soc. Rev. 35 (2006) 1084–1094.
[5] A. Wittstock, J. Biener, J. Erlebacher, M. Baümer, Nanoporous Gold: from an Ancient Technology to a High-tech Material, Royal Society of Chemistry, Cambridge, 2012, p. 252.
[6] Q. Zhang, N. Large, P. Nordlander, H. Wang, Porous Au nanoparticles with tunable plasmon resonances and intense field enhancements for single-particle, SERS J. Phys. Chem. Lett. 5 (2014) 370–374.
[7] A.B. Tesler, B.M. Maoz, Y. Feldman, A. Vaskevich, I. Rubinstein, Solid-state thermal dewetting of just-percolated gold films evaporated on glass: development of the morphology and optical properties, J. Phys. Chem. C 117 (2013) 11337–11346.
[8] J.W. Leem, Y. Yeh, J. Su Yu, Enhanced transmittance and hydrophilicity of nanostructured glass substrates with antireflective properties using disordered gold nanopatterns, Opt. Express 20 (2012) 4056–4066.
[9] L. Qian, W. Shen, B. Das, Bo Shen, G.W. Qin, Alumina coating of ultrafine nanoporous gold at room temperature and their optical properties, Chem. Phys. Lett. 479 (2009) 259–263.
[10] S. Ahl, P.J. Cameron, J. Liu, W. Knoll, J. Erlebacher, F. Yu, A Comparative plasmonic study of nanoporous and evaporated gold films, Plasmonics 3 (2008) 13–20.
[11] C. Vidal, D. Wang, P. Schaaf, C. Hrelescu, T.A. Klar, Optical plasmons of individual gold nanosponges, ACS Photonics 2 (2015) 1436–1442.
[12] M.B. Haddada, J. Blanchard, S. Casale, J.-M. Krafft, A. Vallée, C. Méthivier, S. Boujday, Optimizing the immobilization of gold nanoparticles on functionalized silicon surfaces: amine- vs thiol-terminated silane, Gold Bull. 46 (2013) 335–341.
[13] T. Kameyama, Y. Ohno, T. Kurimoto, K. Okazaki, T. Uematsu, S. Kuwabata, T. Torimoto, Size control and immobilization of gold nanoparticles stabilized in an ionic liquid on glass substrates for plasmonic applications, Phys. Chem. Chem. Phys. 12 (2010) 1804–1811.
[14] W.J. Dressick, C.S. Dulcey, J.H. Georger, J.M. Calvert, Patterning of self-assembled films using lithographic exposure tools, Chem. Mater. 5 (1993) 148–150.
[15] P.A. Schaal, U. Simon, Guided immobilisation of single gold nanoparticles by chemical electron beam lithography, Beilstein J. Nanotechnol. 4 (2013) 336–344.
[16] C.V. Thompson, Solid-state dewetting of thin films, Annu. Rev. Mater. Res. 42 (2012) 399–434.
[17] D. Wang, P. Schaaf, Solid-state dewetting for fabrication of metallic nanoparticles and influences of nanostructured substrates and dealloying, Phys. Status Solidi A 210 (2013) 1544–1551.
[18] D. Wang, R. Ji, P. Schaaf, Formation of precise 2D Au particle arrays via thermally induced dewetting on pre-patterned substrates, Beilstein J. Nanotechnol. 2 (2011) 318–326.
[19] D. Wang, P. Schaaf, Nanoporous gold nanoparticles, J. Mater. Chem. 22 (2012) 5344–5348.
[20] R.N. Viswanath, V.A. Chirayath, R. Rajaraman, G. Amarendra, C.S. Sundar, Ligament coarsening in nanoporous gold: insights from positron annihilation study, Appl. Phys. Lett. 102 (2013) 253101.
[21] M. Fujita, T. Tokunaga, L. Zhang, D. Li, L. Chen, S. Arai, Y. Yamamoto, A. Hirata, N. Tanaka, Y. Ding, M. Chen, Atomic observation of catalyst-induced nanopore coarsening of nanoporous gold, Nano Lett. 14 (2014) 1172–1177.
[22] A. Kosinova, D. Wang, P. Schaaf, O. Kovalenko, L. Klinger, E. Rabkin, Fabrication of hollow gold nanoparticles by dewetting, dealloying and coarsening, Acta Mater. 102 (2016) 108–115.
[23] X.Y. Lang, H. Guo, L.Y. Chen, A. Kudo, J.S. Yu, W. Zhang, A. Inoue, M.W. Chen, Novel nanoporous Au-Pd alloy with high catalytic activity and excellent electrochemical stability, J. Phys. Chem. C 114 (2010) 2600–2603.
[24] J. Snyder, P. Asanithi, A.B. Dalton, J. Erlebacher, Stabilized nanoporous metals by dealloying ternary alloy precursors, Adv. Mater. 20 (2008) 4883–4886.
[25] X. Ge, X. Yan, R. Wang, F. Tian, Y. Ding, Tailoring the structure and property of Pt-decorated nanoporous gold by thermal annealing, J. Phys. Chem. C 113 (2009) 7379–7384.
[26] M.M. Biener, J. Biener, A. Wichmann, A. Wittstock, T.F. Baumann, M. Baeumer, A.V. Hamza, ALD functionalized nanoporous gold: thermal stability, mechanical properties, and catalytic activity, Nano Lett. 11 (2011) 3085–3090.
[27] H. Sadan, W.D. Kaplan, Au-sapphire (0001) solid-solid interfacial energy, J. Mater. Sci. 41 (2006) 5099–5107.
[28] A.P. Warren, T. Sun, B. Yao, K. Barmak, M.T. Toney, K.R. Coffey, Evolution of nanoscale roughness in Cu/SiO_2 and Cu/Ta interfaces, Appl. Phys. Lett. 100 (2012) 024106.
[29] Ph. Buffat, J.-P. Borel, Size effect on the melting temperature of gold particles, Phys. Rev. A 13 (1976) 2287–2298.
[30] S. Jakschik, U. Schroeder, T. Hecht, M. Gutsche, H. Seidl, J.W. Bartha, Crystallization behavior of thin ALD-Al_2O_3 films, Thin Solid Films 425 (2003) 216–220.
[31] R. Katamreddy, R. Inman, G. Jursich, A. Soulet, A. Nicholls, C. Takoudis, Post deposition annealing of aluminum oxide deposited by atomic layer deposition using tris(diethylamino)aluminum and water vapor on Si(100), Thin Solid Films 515 (2007) 6931–6937.
[32] A.H. Tavakoli, P.S. Maram, S.J. Widgeon, J. Rufner, K. van Benthem, S. Ushakov, S. Sen, A. Navrotsky, Amorphous alumina nanoparticles: structure, surface energy, and thermodynamic phase stability, J. Phys. Chem. C 117 (2013) 17123–17130.
[33] S.P. Adiga, P. Zapol, L.A. Curtiss, Atomistic simulations of amorphous alumina surfaces, Phys. Rev. B 74 (2006) 064204.
[34] J. Weissmüller, H.-L. Duan, D. Farkas, Deformation of solids with nanoscale pores by the action of capillary forces, Acta Mater. 58 (2010) 1–13.
[35] L.M. Liz-Marzán, Tailoring surface plasmons through the morphology and assembly of metal nanoparticles, Langmuir 22 (2006) 32–41.
[36] S. Link, M.A. El-Sayed, Shape and size dependence of radiative, non-radiative and photothermal properties of gold nanocrystals, Int. Rev. Phys. Chem. 19 (2000) 409–453.
[37] M.M. Alvarez, J.T. Khoury, T.G. Schaaff, M.N. Shafigullin, I. Vezmar, R.L. Whetten, Optical absorption spectra of nanocrystal gold molecules, J. Phys. Chem. B 101 (1997) 3706–3712.
[38] J.-H. Li, S.-W. Chen, Yi Chou, M.-C. Wu, C.-H. Hsueh, W.-F. Su, Effects of gold film morphology on surface plasmon resonance using periodic P3HT: PMMA/Au nanostructures on silicon substrate for surface-enhanced Raman scattering, J. Phys. Chem. C 115 (2011) 24045–24053.
[39] F. Yu, S. Ahl, A.-M. Caminade, J.-P. Majoral, W. Knoll, J. Erlebacher, Simultaneous excitation of propagating and localized surface plasmon resonance in nanoporous gold membranes, Anal. Chem. 78 (2006) 7346–7350.
[40] M.A. Mahmoud, D. O'Neil, M.A. El-Sayed, Hollow and solid metallic nanoparticles in sensing and in nanocatalysis, Chem. Mater. 26 (2014) 44–58.